



MALAYSIAN JOURNAL OF BIOCHEMISTRY & MOLECULAR BIOLOGY

The Official Publication of The Malaysian Society for Biochemistry & Molecular Biology
(MSBMB)
<http://mjbmb.org>

PUTATIVE TARGET PROTEINS OF THE RIBOSOMAL PROTEIN, RPeL27 IN NASOPHARYNGEAL CARCINOMA CELLS

Edmund Ui-Hang Sim* and Keh-Li Yew

Department of Molecular Biology, Faculty of Resource Science and Technology, Universiti Malaysia Sarawak, Kota Samarahan, Sarawak, Malaysia

*Corresponding Author: uhsim@unimas.my

History

Received: 8th July 2019
Accepted: 22nd December 2019

Keywords:

Nasopharyngeal carcinoma; ribosomal protein; RPeL27; gene knockdown; protein-protein interaction

Abstract

The pathogenesis of nasopharyngeal carcinoma (NPC) is multifactorial and multigenic. Despite the identification of several NPC-associated ribosomal proteins (RPs), the roles of these factors and their interacting partners in NPC tumorigenesis are poorly understood. To date, NPC-associated RP genes are either up or down-regulated in diseased/tumour situation compared to normal condition. The ribosomal protein eL27 (RPeL27) has been known to be over-expressed at both transcript and protein levels in NPC cell lines. This hypothesis was reinforced by our study herein. More importantly, using gene knockdown (RNA interference technique) followed by 2D gel electrophoresis (2D GE) and *in silico* analysis; we revealed 15 proteins that are likely to interact with RPeL27 during situation of NPC tumorigenesis. These include COTL1, MAGOHB, UBE2N, NDPKA, TMED10, PSMB6, CA2, PGAM1, RPeL14, RPeS8, TPI1, PSMA2, RPeL19, GSTP1, and TPM1. Their association with RPeL27 could attribute to gene expression alteration, cell migration disruption and invasion, promotion of cancer cell survival, immune evasion, and genomic instability. Our findings provide new theoretical insights into the mechanism and involvement of RPeL27 in NPC pathogenesis. This is pertinent in understanding the molecular pathogenesis mediated by ribosomal proteins in the malignancy of the nasopharyngeal tissues.

INTRODUCTION

Ribosome is important for protein synthesis in every cell and ribosome biogenesis is well-monitored event in the control of cell growth. Eukaryotic ribosomes, also known as 80S ribosomes, are made up of small and large subunit of ribosomal proteins (RPs). The dysregulation of RPs is often detected in cancer cells. In addition, oncogenes are known to enhance ribosome biogenesis in order to stimulate cancer cell growth [1]. To date, several RPs (*RPeL27*, *RPeL43*, *RPeL41*, *RPuS8*, *RPuS4*, *RPeS31* and *RPuL14*) have been found to be differentially expressed in nasopharyngeal carcinoma (NPC) cells lines relative to non-malignant or normal counterparts [2,3]. *RPeL27*, *RPeL43*, and *RPeL41* were found to be significantly upregulated while *RPuS8*, *RPuS4*, *RPeS31* and *RPuL14* were downregulated significantly in NPC. These findings have suggested some pivotal roles of RPs in NPC pathogenesis. However, despite a demonstration of NPC association on the basis of differential expression, very little to nothing is known with respect to the interactions between RPs and their molecular targets during NPC tumorigenesis. In the case of *RPeL27*, its markedly overexpression in NPC cells [2] was also detected in

hepatocellular carcinoma, liver cancer and, gastric tubular adenoma and carcinoma [4,5,6]. To date, the biological significance of its upregulation in NPC is largely unclear. Herein, we aimed to identify and characterize the proteins that may associate with RPeL27 in the context NPC tumorigenesis. To achieve this, we first verified the overexpression of RPeL27 at transcript and protein levels in 6 NPC cell lines. Subsequently, we knocked down its expression in a representative cell line model to identified possible interacting factors. *In silico* approach was then carried out to assess logical protein-protein interaction between RPeL27 and its putative partners.

MATERIALS AND METHODS

Cell lines and Culture

Six NPC cell lines (HONE-1, SUNE-1, HK1, TW01, TW04 and C666-1) were used in this study. The non-malignant nasopharyngeal epithelial cell line (NP69) was used as a control. All these originated from the University of Hong Kong, with permission for use granted by Professor George S. W. Tsao. The NPC cell lines were cultured in RPMI-1640 (Gibco, Life Technologies, USA) with 10% (v/v) fetal bovine serum, 2mM L-

glutamine, and 100 U/mL penicillin-streptomycin (Gibco, USA). NP69 was cultured in defined keratinocyte serum free medium (Invitrogen, USA) containing 0.2ng/mL growth factors, 5% heat-activated FBS with 100 U/mL penicillin-streptomycin. All cell lines were cultured in a humidified incubator (37°C, 5% CO₂) and harvested at 80% growth confluence.

Total RNA Extraction and cDNA Synthesis

Total RNA extraction was carried out using Trizol method (Invitrogen, USA). Extracted RNA was treated with RQ1 RNase-Free DNase (Promega, USA). First strand cDNA synthesis was by Moloney Murine Leukemia Virus (MML-V) reverse transcriptase (Promega, USA), and done according to manufacturer's protocol.

Quantitative Polymerase Chain Reaction (qPCR)

For qPCR analysis, 1 µl (80ng) of the first strand cDNA template was added to a final volume of 12.5 µl with 1X QuantiNova SYBR Green PCR Master Mix (Qiagen, USA) and 0.56 µM of forward and reverse primers each. The glyceraldehyde-3-phosphate dehydrogenase (*GAPDH*) (NM_002046.5) (forward: 5'-CTGGGCTACACTGAGCACC-3'; reverse: 5'-AAGTGGTCG TTAGGGCAATG-3') served as a reference gene for normalization of the target gene cDNA input. Amplification was carried out and analyzed using the Rotor-Gene™ 6000 Rotary Analyzer (Qiagen, USA), and the Rotor-Gene™ 6000 software Version 2.3.3 (Qiagen, USA). The preformation of quantitative gene amplification was with initial denaturation at 95 °C for 2 min followed by 40 cycles of denaturation at 95°C for 5 sec, annealing at 60 °C for 10 sec, and extension at 72 °C for 10 sec. Triplicate analysis was implemented. The PCR efficiency and primers compatibility of each gene of interest and reference gene (*GAPDH*) were validated using standard curve method [10]. Melting curve analysis with the temperature range of 55 to 99°C for each run was done to ascertain specificity of PCR amplification. The validation of primer efficiency was determined from the slope of calibration curve as follows:

$$\text{Amplification efficiency} = [10^{-1/\text{slope}}] - 1$$

Amplification efficiency of target and reference gene are both at 1.00 (100%). The Correlation Coefficient (R²) value for each gene (determined from the calibration curve) is more than 0.90 (90%), and the *m* values are within the range of -3.6 and -3.1. A standard curve was then plotted and the absolute value of the slope (*m*) of the curve is less than 0.1 thus validated the primers' compatibility and PCR efficiency.

Western Blot

Total protein extraction was done using lysis buffer [radioimmunoprecipitation assay (RIPA) buffer with 1mM phenylmethanesulfonylfluoride (PMSF) protease inhibitor (Roche Applied Science, Switzerland)]. 20 µg of each sample in 2X Laemmli sample buffer (Bio-rad, Germany) was loaded into wells of Sodium Dodecyl Sulfate (SDS) polyacrylamide gel along with the PageRuler™ Prestained protein ladder (ThermoScientific, USA). The primary antibodies used were rabbit primary antibody against RPeL27 (Abcam, UK) and beta (β)-actin (ACTB) (Abcam, UK), while the secondary antibody was donkey anti-rabbit Horse- Radish Peroxide (HRP) conjugated secondary antibody (Santa Cruz Biotechnology, USA). ACTB served as a loading control. Image documentation was via

ImageQuant TL instrument (GE Healthcare, UK) and ImageQuant TL software. The band intensities were evaluated using ImageJ software (National Institutes of Health, NIH). Triplicate analysis was performed.

RNA interference (RNAi)

The NPC cell line, HK1 was transiently transfected with 10 nM of Dicer-substrate RNA, DsiRNA #1 (5'-CGCCAAGAGAUCAAAGAUAAAUAUC-3') using lipofectamine™ 2000 (Invitrogen, USA). Hypoxanthine guanine phosphoribosyltransferase 1 (*HPRT1*) (5'GCCAGACUUUGUUGGAUUUGAAAT T-3') served as a positive control for transfection efficiency. In addition, negative control (5'-CGUUAUUCGCGUAUAAUACGC GUAT-3'), mock-transfected, TYE 63 fluorescence transfection control and untreated HK1 were included to ascertain knockdown efficiency. The cells were extracted after 48 hours to assay the gene knockdown efficiency using reverse transcriptase PCR (RT-PCR) and western- blot analysis. 2D gel electrophoresis was employed for the protein expression analysis. Protein identification was by liquid chromatography-mass spectrometry (LC-MS) method.

Gene ontology (GO) term enrichment analysis

The bioinformatics enrichment web tool known as Database for Annotation, Visualization and Integrated Discovery (DAVID, <http://david.abcc.ncifcrf.gov/>) was used in order to understand protein functional annotation analysis [7] with the cut-off criterion at *p*<0.05.

Protein-protein interaction (PPI) Prediction

The 3-dimensional (3D) model of RPeL27 was built based on homology modelling strategy by using the SWISS-MODEL workplace [8,9,10]. RPeL27 was comparatively modelled with template structures using the result from target- template alignment and evaluated using Qualitative Model Energy Analysis (QMEAN) [11] and PROCHECK tools [12] to access model quality and structural assessment respectively. Computational docking of the comparative 3D-model of RPeL27 with its partners was performed via the ClusPro 2.0 application [13]. Docked complexes were evaluated based on cluster and energy score, and examined using SWISS_Pdb Viewer v4.1 [14]. The root mean square deviation (RMSD) was computed to predict the potential interaction sites based on interface contact residues (<5Å).

RESULTS AND DISCUSSION

The gene and protein expression data show significant overexpression of RPeL27 in NPC cell lines compared to NPE cell line (Figure 1). This confirms its upregulation in NPC cell lines [2], and extends the validity of the expression trend in two other cell lines, TW04 and C666-1. More importantly, we have demonstrated its overexpression (transcript and protein) in a Type IIB, undifferentiated non-keratinized NPC cell line that is Epstein-Barr virus (EBV) positive, C666-1. The upregulated of RPeL27 in C666-1 has never been reported before this. EBV-positive Type IIB NPC is the predominant type of NPC. Our findings imply a pivotal role of RPeL27 in NPC pathogenesis.

Results of RPeL27 knockdown show reduced RPeL27 expression in HK1 cell line compared to the control, with DsiRNA #1 having the best outcome (Figure 2D). The *RPeL27* transcript was decreased to 28% (*p*<0.0001) by DsiRNA #1 while the band intensities for negative control, mock-transfected control

and untransfected control remained unaffected (**Figure 2A**). Positive control represented by *HPRT1* expression was suppressed to 19% ($p<0.01$) under the transfection of 10 nM of HPRT-S1 positive control duplex (**Figure 2B**).

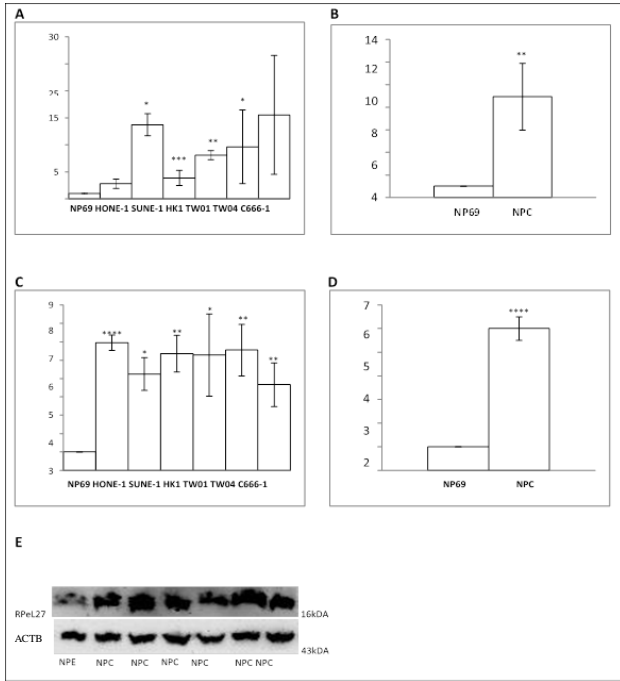


Figure 1. RPeL27 overexpression in NPC cell lines at both transcript and protein level. **a:** Relative *RPeL27* transcript expression in NPC cell lines compared to NPE. **b:** Cumulative fold change of *RPeL27* transcript expression in NPC cell lines versus NPE. **c:** Relative RPeL27 protein expression in NPC cell lines compared to NPE. **d:** Cumulative fold change of RPeL27 protein expression in NPC cell lines versus NPE. **e:** The protein levels of RPeL27 in NPC cell lines determined by western blot. (* $p<0.05$, ** $p<0.01$, *** $p<0.001$, **** $p<0.0001$)

The reduction of more than 80% in the control test tallied with more than 80% of cells being transfected (**Figure 2C**), thus validating our knockdown analysis. From the 2D gel electrophoresis assay, comparative analysis of HK1 cells treated with DsiRNA#1 and untreated cells revealed 10 spots with observable differential protein expressions (**Figure 3**). Spots 1 to 9 show reduced intensity, while Spot 10 has higher intensity in the test compared to control. Protein identification of these spots via LCMS reveals 15 different proteins (**Table 1**). Spots 4, 6, and 8 consist of two types of protein each, and Spot 7 has three types. All other spots comprise a single type of protein. Differential expressions of these proteins in association to deregulated (suppressed) expression of RPeL27 in the context of an NPC cell model are reported for the first time here. The expression of NDPKA (Spot 4), CA2 (Spot 6) and GSTP1 (Spot 9) have been previously reported in NPC, and found to be upregulated in NPC tissues compared to normal nasopharyngeal epithelial tissues [15,16,17].

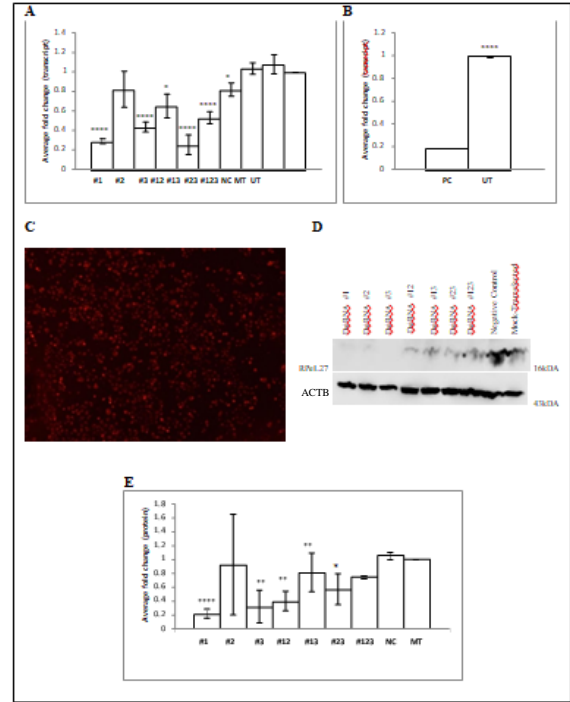


Figure 2. Verification of RPeL27-knockdown in HK1 cells after DsiRNA transfection. **a, b:** Knockdown efficacy assessed via *RPeL27* and *HPRT1* transcript level in HK1 by RT-PCR. **c:** Transfection efficiency visualized 24 hours post-transfection of 10nm transfection control under fluorescence microscopy. **d:** The protein levels of RPeL27 in RNAi experiment with different treatments determined by western blot analysis. The RPeL27 protein level in RPeL27-knockdown HK1 measured by western blot (* $p<0.05$, ** $p<0.01$, *** $p<0.001$, **** $p<0.0001$) (NC: negative control; MT: mock-transfected; UT: untreated; PC: positive control)

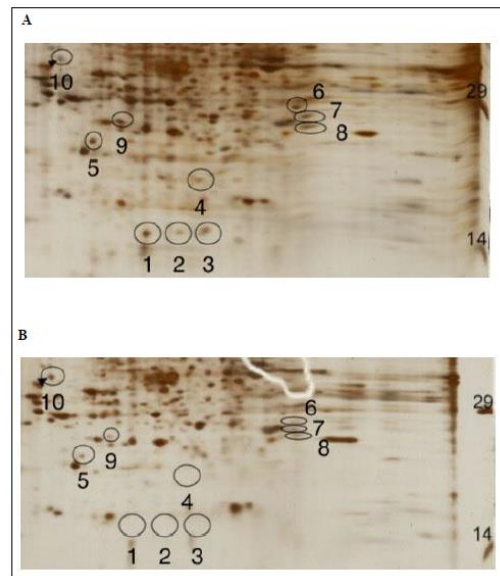


Figure 3. 2D gel images to access the proteins affected by RPeL27-knockdown in HK1. **A)** protein expressions in untreated HK1. **B)** protein expressions in RPeL27- knockdown HK1. Spot 1 to 10 were circled and labelled accordingly in both images.

Results of GO-terms enrichment analysis on biological processes related to the protein-protein interactions among these proteins reveals 23 biological processes involved in cell growth and proliferation (**Table 2**).

Table 2. GO-term enrichment analysis (biological process only) of proteins identified by LCMS on 2D gels

Term	Proteins	p-value
GO:0000184~nuclear-transcribed mRNA catabolic process, nonsense-mediated decay	MAGOHB, RPL14, RPeL19, RPeL27 & RPeS8	5.3E-6
GO:0006614~SRP-dependent cotranslational protein targeting to membrane	RPeL14, RPeL19, RPeL27 & RPeS8	1.1E-4
GO:0019083~viral transcription	RPeL14, RPeL19, RPeL27, RPeS8	1.8E-4
GO:0006413~translational initiation	RPeL14, RPeL19, RPeL27 & RPeS8	3.3E-4
GO:0006364~rRNA processing	RPeL14, RPeL19, RPeL27 & RPS8	1.2E-3
GO:0006412~translation	RPeL14, RPeL19, RPeL27 & RPS8	2.0E-3
GO:0002223~stimulatory C-type lectin receptor signaling pathway	PSMA2, PSMB6 & UBE2N	5.0E-3
GO:1904706~negative regulation of vascular smooth muscle cell proliferation	GSTP1 & TPM1	8.1E-3
GO:0050852~T cell receptor signaling pathway	PSMA2, PSMB6 & UBE2N	9.6E-3
GO:0038095~Fc-epsilon receptor signaling pathway	PSMA2, PSMB6 & UBE2N	1.4E-2
GO:0061621~canonical glycolysis	PGAM1 & TPI1	2.6E-2
GO:0006096~glycolytic process	PGAM1 & TPI1	3.4E-2
GO:0006094~gluconeogenesis	PGAM1 & TPI1	4.4E-2
GO:0051603~proteolysis involved in cellular protein catabolic process	PSMA2 & PSMB6	4.8E-2
GO:0006521~regulation of cellular amino acid metabolic process	PSMA2 & PSMB6	5.0E-2
GO:0002479~antigen processing and presentation of exogenous peptide antigen via MHC class I, TAP-dependent	PSMA2 & PSMB6	6.2E-2
GO:0038061~NIK/NF-kappaB signaling	PSMA2 & PSMB6	6.5E-2
GO:0051436~negative regulation of ubiquitin- protein ligase activity involved in mitotic cell cycle	PSMA2 & PSMB6	7.0E-2
GO:0051437~positive regulation of ubiquitin- protein ligase activity involved in regulation of mitotic cell cycle transition	PSMA2 & PSMB6	7.4E-2
GO:0031145~anaphase-promoting complex- dependent catabolic process	PSMA2 & PSMB6	7.7E-2
GO:0001822~kidney development	CA2 & TMED10	8.4E-2
GO:0060071~Wnt signaling pathway, planar cell polarity pathway	PSMA2 & PSMB6	8.9E-2
GO:0043488~regulation of mRNA stability	PSMA2 & PSMB6	9.9E-2

Pathways commonly associated with oncogenesis, such as the NF-kappaB, and Wnt signalling are evident. In explore possible interaction between RPeL27 with each of the 15 proteins, computational molecular docking analysis was performed. 3D models of all proteins were first constructed (**Figure 4**). Quality scrutiny of the models via QMEAN6 Score (**Table 3**) and PROCHECK (**Table 4**) assessment confirmed amenability for docking simulation. Only the top dock models (**Figure 5**) with plausible docking scenario (interface contact residues within 5Å), were interpreted for protein-protein interaction (Tables 5-6) with specific functional interaction sites for each dock complex detailed (**Table 7**). On the basis of the expected biological processes (**Table 2**), and the docking results (Tables 5-7, Figure 5), an extrapolated pathway of NPC pathogenesis mediated by

RPeL27 can be explained (**Figure 6**). Basically, during NPC tumourigenesis, the dysregulated expression *RPeL27* could associate directly with at least 15 other proteins (COTL1, MAGOHB, UBE2N, NDPKA, TMED10, PSMB6, CA2, PGAM1, RPeL14, RPeS8, TPI1, PSMA2, RPeL19, GSTP1, and TPM1) to alter gene expression, disrupt cell migration and invasion, promote cancer cell survival, enable immune evasion, and contribute to genomic instability.

Table 1. Protein identification by LCMS of the spots showing differential intensity in the 2D gel images

Spot	Protein	NCBI Accession	MW (Da)	Ion score /p-value
1	Coactosin-like protein (COTL-1)	NP_066972.1	15935	346/<0.05
2	Protein mago nashi homolog 2 (MAGOHB)	NP_060518.1	17265	75/<0.05
3	Ubiquitin-conjugating enzyme E2N (UBE2N)	NP_003339.1	17127	135/<0.05
	Nucleoside diphosphate kinase A (NDPKA)	NP_937818.1	17138	99/<0.05
4	Transmembrane emp24 domain-containing protein 10 (TMED10)	NP_006818.3	24960	68/<0.05
5	Proteasome subunit beta type-6 (PSMB6)	NP_002789.1	25299	119/<0.05
6	Phosphoglycerate mutase (PGAM1)	NP_002620.1	28817	186/<0.05
	Carbonic anhydrase (CA2)	NP_000058.1	29228	43/<0.05
	Triosephosphate isomerase (TPI1)	NP_000356.1	22857	149/<0.05
7	40S ribosomal protein S8 (RPeS8)	NP_001003.1	21866	140/<0.05
	60S ribosomal protein L14 (RPeS14)	NP_003964.3	13772	53/<0.05
8	Proteasome subunit alpha type-2 (PSMA2)	NP_002778.1	25882	173/<0.05
	60S ribosomal protein L19 (RPeL19)	NP_000972.1	23233	61/<0.05
9	Gluthione S-transferase P (GSTP1)	NP_000843.1	23341	116/<0.05
10	Tropomyosin alpha-1 chain (TPM1)	NP_001018008.1	32689	283/<0.05

Table 3. Raw scores of the 6 structural terms of each protein 3D-model with their respective QMEAN6 score

Model	C_beta interaction energy	All-atom pairwise energy	Solv. energy	Torsion angle energy	Secondary structure agreement	Solvent accessibility agreement	QMEAN6 score
RPeL27	0.00	-0.001	-0.71	-0.14	0.62	0.67	0.69
COTL1	-0.01	-0.03	-0.78	-0.15	0.63	0.59	0.71
MAGOHB	-0.01	-0.03	-0.80	-0.82	0.69	0.61	0.72
UBE2N	-0.01	-0.02	-0.80	-0.38	0.81	0.59	0.81
NDPKA	-0.02	-0.03	-0.74	-0.22	0.63	0.63	0.75
TMED10	-0.01	-0.03	-0.66	-0.39	0.88	0.57	0.79
PSMB6	-0.01	-0.02	-0.70	-0.19	0.74	0.58	0.73
CA2	-0.02	-0.02	-0.61	-0.30	0.61	0.88	0.80
PGAM1	-0.02	-0.02	-0.76	-0.26	0.62	0.61	0.75
RPL14	-0.00	-0.02	-0.82	-0.15	0.67	0.58	0.70
RPS8	0.00	-0.01	-0.73	0.00	0.49	0.67	0.63
TPI1	-0.01	-0.02	-0.69	-0.25	0.71	0.62	0.74
PSMA2	-0.01	-0.02	-0.69	-0.04	0.69	0.61	0.69
RPL19	-0.02	-0.04	-0.90	-0.15	0.61	0.66	0.75
GSTP1	-0.01	-0.02	-0.82	-0.33	0.50	0.86	0.80
TPM1	-0.04	-0.08	-1.21	-0.19	0.95	0.70	0.88

Table 4. PROCHECK statistical data checks stereochemical quality for each protein generated from SWISS-MODEL

Model	Core region (%)	Allowed region (%)	Generously allowed region (%)	Disallowed region (%)	Bad contacts	G-factor	Planar region (%)
RPeL27	95.0	3.3	1.7	0.0	0	-0.23	83.0
COTL1	94.1	5.0	0.0	0.8	0	-0.10	94.1
MAGOHB	92.2	6.2	1.6	0.0	0	-0.20	88.9
UBE2N	90.7	9.3	0.0	0.0	0	-0.11	94.5
NDPKA	93.7	5.6	0.0	0.8	0	-0.12	87.7
TMED10	92.9	5.9	0.0	1.2	0	-0.11	91.4
PSMB6	91.1	8.9	0.0	0.0	0	-0.13	83.1
CA2	89.8	9.6	0.5	0.0	1	-0.13	92.9
PGAM1	89.5	10.5	0.0	0.0	0	-0.14	90.7
RPL14	96.1	3.1	0.8	0.0	0	-0.14	86.5
RPS8	87.9	8.8	1.6	1.6	0	-0.09	88.6
TPI1	92.9	7.1	0.0	0.0	0	-0.11	88.3
PSMA2	88.9	8.4	0.5	2.1	0	-0.35	78.2
RPL19	89.9	7.7	1.8	0.6	0	-0.26	91.4
GSTP1	95.5	2.8	1.7	0.0	0	0.00	89.3
TPM1	99.6	0.4	0.0	0.0	0	-0.10	97.5

Table 5. ClusPro scores of RPeL27 dock models

Dock Model	ClusPro scores			RMSD (Å)
	Cluster size	Center free energy (kcal/mol)	Lowest free energy (kcal/mol)	
RPeL27_COTL1	107	-497.4	-551.8	0.91
RPeL27_MAGOHB	140	-681.6	-767.5	0.85
RPeL27_UBE2N	154	-644.1	-810.6	0.89
RPeL27_NDKPA	99	-813.1	-919.2	0.88
RPeL27_TMED10	269	-650.0	-778.0	0.91
RPeL27_PSMB6	126	-771.6	-852.5	0.95
RPeL27_CA2	148	-661.3	-699.4	0.90
RPeL27_PGAM1	212	-742.9	-891.2	0.92
RPeL27_RPL14	141	-629.3	-658.1	0.86
RPeL27_RPS8	175	-523.8	-629.5	0.84
RPeL27_TPI1	123	-568.8	-711.6	0.89
RPeL27_PSMA2	171	-734.8	-869.4	0.91
RPeL27_RPL19	130	-522.5	-604.7	0.87
RPeL27_GSTP1	108	-632.2	-801.9	0.88
RPeL27_TPM1	160	-738.6	-832.0	0.93

Whether these events are causes or consequences of malignancy remains to be further investigated. Therefore, functional studies of these 15 proteins in association with RPeL27 under the context of NPC oncogenesis are required to resolve these queries. Nevertheless, our findings are the first to provide both empirical and logical data on involvement and explanation of *RPeL27* gene in molecular pathogenesis nasopharyngeal cancer.

Table 6. Potential interaction sites based on interface contact residues

Protein	Interface contact residues (<5Å)
RPeL27	Gly2, Phe4, Leu12, Val13, Leu14, Ala15, Gly16, Ser19, Gly20, Asn78, His79, Leu80, Met81, Pro82, Thr83, Arg84, Tyr85, Trp129, Leu134, Arg135, Phe136
COTL1	Glu8, Ala9, Arg11, Ala12, Ala13, Asn15, Leu16, Asp19, Asp20, Gly21, Ser22, Ala23, Val24, Trp26, Pro38, Gly39, Glu40, Gln41, Gly42, Ala43, Glu44, His47, Leu14, Ala15, Gly16, Arg17, Tyr18, Ser19, Gly20, Arg21, Asp47, Arg48, Arg51, Met57, Lys61, Arg65, Lys69, Lys133, Leu134, Arg135, Phe136
RPeL27 MAGOHB	Ala4, Ser5, Glu70, Ile71, Thr72, Lys73, Glu74, Asp75, Asp76, Ala77, Leu88, Trp79, Asp96, Glu97, His98, Ile99, Phe101, Ser115, Lys116, Asp117, Pro118, Glu119, Gly120, Arg122
RPeL27	Gly2, Phe4, Leu12, Val13, Leu14, Ala15, Ser19, Gly20, Tyr77, Asn78, His79, Leu80, Met81, Pro82, Arg84, Tyr85, Trp129, Lys133, Leu134, Arg135, Phe136
UBE2N	Arg14, Pro19, Val20, Pro21, Gly22, Ala40, Gly41, Pro42, Gln43, Asp44, Ser45, Asp89, Ser96, Ala98, Leu99, Gln100, Arg102, Thr103, Val104, Leu106, Ser107, Gln109, Ala110, Leu112, Ser113, Ala114, Asn116, Asp118, Asp119, Pro120
RPeL27 NDPKA	Gly2, Phe4, Leu12, Val13, Leu14, Ala15, Ser19, Gly20, Tyr38, Asn78, His79, Met81, Pro82, Thr83, Arg84, Tyr85, Trp129, Leu134, Arg135, Phe136 Val46, Ile50, Lys51, Glu54, Phe58, Arg59, Leu60, Val61, Gly62, Leu63, Lys64, Phe65, Val99, Trp103, Glu162, Glu163, Val165, Asp166, Tyr167, Thr168, Ser169, Cys170, Ala171, Trp174
RPeL27 TMED10	Gly16, Arg17, Tyr18, Ser19, Gly20, Arg21, Asp47, Arg48, Tyr49, Pro50, Arg51, Lys52, Arg65, Lys69, Lys133, Leu134, Arg135, Phe136 His49, Lys50, Asp51, Lys57, Asp78, Ser79, Ala80, Gly81, His82, Ile83, Leu84, Thr98, Thr99, Glu100, Asp101, Tyr102, Asp103, Met104,
RPeL27 PSMB6	Leu12, Val13, Leu14, Ala15, Gly16, Ser19, Gly20, Arg21, Lys22, Asn78, His79, Met81, Thr83, Arg84, Tyr85, Trp129, Gln132, Lys133, Leu134, Arg135, Phe136 Pro70, Ile71, His72, Asp73, Arg74, Phe76, Thr94, Tyr95, Gln96, Gly98, Phe99, Ser101, Ile102, Glu103, Asn105, Glu106, Pro107, Tro137, Pro139, Glu215, Ser216, Gly217, Val218, Arg220
RPe27 CA2	Leu12, Val13, Leu14, Gly16, Arg17, Tyr18, Ser19, Gly20, Arg21, Lys22, Asp47, Arg48, Arg51, Lys69, Met81, Trp129, Gln132, Lys133, Leu134, Arg135, Phe136
RPeL27 PGAM1	Met1, Ser2, His3, His4, Trp5, Gly6, Tyr7, Gly8, Lys9, His10, Asn11, Gly63, His64, Lys169, Phe230, Asn231, Glu233, Gly234, Glu235, Pro236, Glu237, Glu238, Leu239, Met240, Val241, Asp242, Asn243, Phe259
RPeL27 RPS8	Gly2, Phe4, Leu12, Leu14, Tyr77, Asn78, His79, Leu80, Met81, Pro82, Thr83, Arg84, Tyr85, Trp129, leu134, Arg135, Phe136 His35, Lys61, Ile64, Arg65, Leu65, Trp68, Leu71, Asp72, Ala73, Asp75, Met77, Trp78, Leu79, Pro80, Val81, Val82, Arg83
RPeL27 TPI1	Gly2, Lys3, Phe4, Met5, Leu12, Val13, Leu14, Ala15, Ser19, Gly20, Asp30, Asp31, Pro37, Tyr38, Ser39, Asn76, Tyr77, Asn78, His79, Leu80, Met81, Pro82, Thr83, leu134, Arg135, Phe136 Asn7, Trp8, Lys10, Arg11, Arg12, Lys13, Thr14, Lys17, Arg18, Lys19, Pro20, Tyr21, His22, Lys23, Arg25, Tyr27, Glu28, Arg49
RPeL27 PSMA2	Gly2, Phe4, Leu12, Val13, Leu14, Gly20, Asn78, His79, Met81, Pro82, leu134, Arg135, Phe136 Met15, Thr46, Ala47, Ala74, Phe75, Thr76, Glu78, Ser97, Glu98, Arg99, His101, Val102, Phe103, Gly104, Glu105, Lys131, Leu132, Asp133, Val168, Ile171, Gly172
RPeL27 PSMA2	Leu12, Val13, Leu14, Ala15, Gly16, Ser19, Gly20, Arg51, His79, Met81, Arg84, Tyr85, Lys128, Trp129, Gln132, Lys133, Leu134, Arg135, Phe136

	Lys176, Arg177, Leu182, Glu185, Asp186, Ile188, His189, Thr190, Ile192, Leu193, Lys196, Glu197, Gly201, Gln202, Met203, Glu205, Asp206, Ile108, Val210, Leu221, Pro223, Thr224, Glu225, Val226
RPeL27	Leu12, Val13, Leu14, Gly20, Lys22, Tyr77, Asn78, His79, Leu80, Met81, Pro82, Thr83, Arg84, Trp129, leu134, Arg135, Phe136
RPL19	Arg103, Arg107, Arg110, Glu111, Lys113, Arg117, His118, Tyr120, His121, Ser122, Tyr124, Leu125, Lys128
RPeL27	Gly2, Phe4, Lys6, Lys9, Leu14, Asp30, Ser39, Asn76, Tyr77, Asn78, Leu80, Met81, Pro82,
GSTP1	Thr83, Arg84, lys133, leu134, Arg135, Phe136
	Leu49, Tyr50, Asp58, Gly59, Asp60, Leu61, Thr62, Leu63, Tyr64, Gln65, Thr68, Arg71, His72, Arg75, Tyr80, Gly81, Lys82, Asp83, Gln84, Ala87, Ala88, Asp91, Asp95
RPeL27	Leu14, Ala15, Gly16, Arg17, Tyr18, Ser19, Gly20, Arg21, Asp47, Arg48, Tyr49, Arg51, Met57,
TPM1	Lys61, Lys64, Arg65, lys133, leu134, Arg135, Phe136
	Tyr162, Glu163, Val165, Ala166, Arg167, Leu169, Val170, Ile171, Glu173, Ser174, Leu176, Glu177, Glu180, Glu181, Glu184, Leu185, Glu187, Gly188

RPeL27_RPeS8, **K**) RPeL27_TPI1, **L**) RPeL27_PSMA2, **M**) RPeL27_RPeL19 (overall view), **N**) RPeL27_RPeL19 (enlarged view), **O**) RPeL27_GSTP1, **P**) RPeL27_TPM1 (overall view), and **Q**) RPeL27_TPM1 (enlarged view)

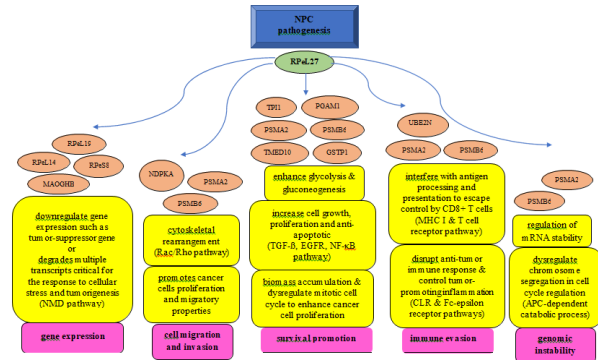


Figure 6. RPeL27 in NPC pathogenesis

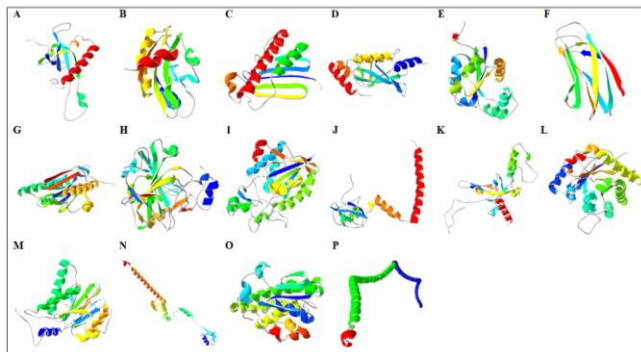


Figure 4. Ribbon (secondary structure) representation of 3-dimensional (3D) model for each protein. These models were rendered by SWISS-Pdb viewer v4.1. Each model is coloured from the N-terminal (blue) to the C-terminal (red). a: RPeL27, b: COTL1, c: MAGOHB, d: UBE2N, e: NDPKA, f: TMED10, g: PSMB6, h: CA2, i: PGAM1, j:RPeL14, k:RPeS8, l: TPI1, m: PSMA2, n: RPeL19, o: GSTP1, and p: TPM1

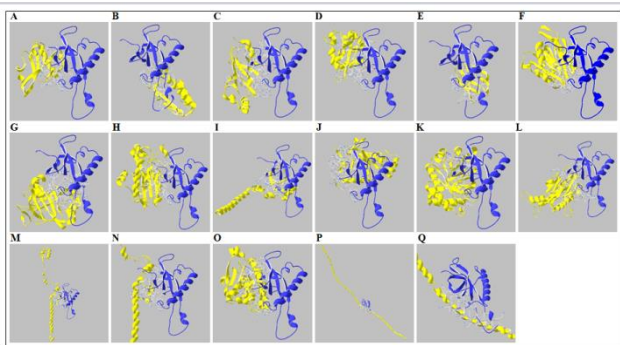


Figure 5. RPeL27-protein docked complex. Blue colored ribbon indicates the RPeL27 protein while the yellow colored ribbon indicates the respective protein. The wireframe illustrates the interface contact residues that are close to another chain (<5Å), depicts the potential interaction site. A) RPeL27_COTL1 B) RPeL27_MAGOHB, C) RPeL27_UBE2N, D) RPeL27_NDPKA, E) RPeL27_TMED10, F) RPeL27_PSMB6, G) RPeL27_CA2, H) RPeL27_PGAM1, I) RPeL27_RPeL14, j) RPeL27_RPeS8, k) RPeL27_TPI1, l) RPeL27_PSMA2, m) RPeL27_RPeL19, n) RPeL27_GSTP1, o) RPeL27_TPM1, p) RPeL27_TPM1, q) RPeL27_TPM1

Table 7. Pfam search assay of each protein target sequence to determine their protein families and domains classification

Protein	Description	Accession	Residues position	Domain E-value
RPeL27	Ribosomal L27e protein family	PF01777.18	52-136	4.2e-39
	KOW motif	PF00467.29	7-40	9.7e-06
COTL1	Cofilin/tropomyosin-type actin-binding protein	PF00241.20	10-128	7.2e-20
MAGOHB	Magi nashi protein	PF02792.14	7-148	2.5e-78
UBE2N	Ubiquitin-conjugating enzyme	PF00179.26	7-144	8.2e-48
NDPKA	Nucleoside diphosphate kinase	PF00334.19	30-164	3.4e-55
TMED10	Emp24/gp25L/p24 family/GOLD	PF01105.24	31-213	1.4e-47
PSMB6	Proteasome subunit	PF00227.26	31-213	1.1e-45
CA2	Eukaryotic-type carbonic anhydrase	PF00194.21	4-258	7.2e-99
			6-138	1.9e-31
PGAM1	Histidine phosphatase superfamily	PF00300.22	134-227	9.3e-06
RPL14	Ribosomal protein L14	PF01929.17	46-120	5.2e-30
RPS8	Ribosomal protein S8e	PF01201.22	1-190	1.7e-57
TPI1	Triosephosphate isomerase	PF00121.18	7-245	1.8e-86
	Proteasome subunit	PF00227.26	29-213	3.1e-60
PSMA2	Proteasome subunit A N-terminal signature	PF10584.9	6-28	4.9e-10
RPL19	Ribosomal protein L19e	PF01280.20	3-146	1.0e-65
	Glutathione S-transferase, C-terminal domain	PF14497.6	98-197	1.6e-15
GSTP1	Glutathione S-transferase, N-terminal domain	PF02798.20	4-75	3.0e-06
TPM1	Tropomyosin	PF00261.20	48-284	2.3e-97

ACKNOWLEDGEMENTS

This research was supported by the Ministry of higher Education, Malaysia by the Fundamental Research Grant Scheme [FRGS/ST03(02)/1299/2015(16)].

CONFLICT OF INTEREST

The authors declare that there is no conflict of interests regarding the publication of this manuscript.

transferase-Pi protein in nasopharyngeal carcinoma. *Hum Pathol.* **32**(11),1240-1244.

REFERENCES

- 1 Ciarmatori, S., Scott, P.H., Sutcliffe, J.E., McLees, A., Alzuherri, H.M., Dannenberg, J.H., et al. (2001) Overlapping functions of the pRb family in the regulation of rRNA synthesis. *Mol Cell Biol.* **21**(17), 5806–5814.
- 2 Sim, E.U., Chan, S.L., Ng, K.L., Lee, C., and Narayanan, K. (2016) Human ribosomal proteins RPeL27, RPeL43, and RPeL41 are upregulated in nasopharyngeal carcinoma cell Lines. *Dis Markers* **ISSN 0278-0240**, 1-7.
- 3 Sim, E.U., Ng, K.L., Lee, C.W., and Narayanan, K. (2017) The uS8, uS4, eS31, and uL14 ribosomal protein genes are dysregulated in nasopharyngeal carcinoma cell lines. *Biomed Res Int.* **2017**, 1-8.
- 4 Kondoh, N., Shuda, M., Tanaka, K., Wakatsuki, T., Hada, A., and Yamamoto, M. (2001) Enhanced expression of S8, L12, L23a, L27 and L30 ribosomal protein mRNAs in human hepatocellular carcinoma. *Anticancer Res.* **21**(4A), 2429-2433.
- 5 Zhang, P.J., Wei, R., Wen, X.Y., Ping, L., Wang, C.B., Dong, Z.N., et al. (2013) Gene expression profiling of peripheral blood cells of patients with hepatocellular carcinoma. *Cell Biol Int.* **36**(9), 803-309.
- 6 De, Giorgi, V., Buonaguro, L., Worschech, A., Tornesello, M.L., Izzo, F., Marincola, F.M., et al. (2013) Molecular signatures associated with HCV-induced hepatocellular carcinoma and liver metastasis. *PLoS One* **8**(2), e56153.
- 7 Huang da, W., Sherman, B.T., and Lempicki, R.A. (2009) Systematic and integrative analysis of large gene lists using DAVID bioinformatics resources. *Nat Protoc.* **4**(1), 44- 57.
- 8 Arnold, K., Bordoli, L., Kopp, J., and Schwede, T. (2006) The SWISS-MODEL workplace: a web-based environment for protein structure homology modelling. *Bioinformatics* **22**(2), 195-201.
- 9 Bordoli, L., Kiefer, F., Arnold, K., Benkert, P., Battey, J., and Schwede, T. (2009) Protein structure homology modeling using SWISS-MODEL workspace. *Nat Protoc.* **4**(1), 1-13.
- 10 Biasini, M., Bienert, S., Waterhouse, A., Arnold, K., Studer, G., Schmidt, T., et al. (2014) SWISS-MODEL: modelling protein tertiary and quaternary structure using evolutionary information. *Nucleic Acids Res.* **42**, W252-258.
- 11 Benkert, P., Biasini, M., and Schwede, T. (2011) Towards the estimation of the absolute quality of individual protein structure models. *Bioinformatics* **27**(3), 343-350.
- 12 Laskowski, R.A., MacArthur, M.W., Moss, D.S., and Thornton, J.M. (1993). PROCHECK: a program to check the stereochemical quality of protein structures. *J. Appl. Cryst.* **26**(2), 283- 291.
- 13 Comeau, S.R., Gatchell, D.W., Vajda, S., and Camacho, C.J. (2004) ClusPro: an automated docking and discrimination method for the prediction of protein complexes. *Bioinformatics* **20**(1), 45-50.
- 14 Guex, N., and Peitsch, M.C. (1997) SWISS-MODEL and the Swiss-PdbViewer: an environment for comparative protein modeling. *Electrophoresis* **18**(15), 2714-2723.
- 15 Cheng, A.L., Huang, W.G., Chen, Z.C., Peng, F., Zhang, P.F., Li, M.Y., et al. (2004) Identification of novel nasopharyngeal carcinoma biomarkers by laser capture microdissection and proteomic analysis. *Clin Cancer Res.* **14**(2), 435-445.
- 16 Luo, Y., Mok, T.S., Lin, X., Zhang, W., Cui, Y., Guo, J., et al. (2017) SWATH-based proteomics identified carbonic anhydrase 2 as a potential diagnosis biomarker for nasopharyngeal carcinoma. *Sci Reports* **7**(41191), 1-11.
- 17 Chen, C.L., Sheen, T.S., Luo, I.U., and Huang, A.C. (2001) Expression of multidrug resistance 1 and glutathione-S-